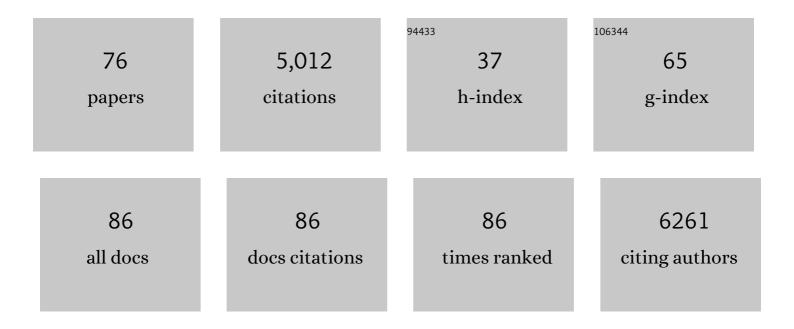
List of Publications by Year in descending order

Source: https://exaly.com/author-pdf/6744771/publications.pdf Version: 2024-02-01



RDUNO WERED

#	Article	IF	CITATIONS
1	Role of sex hormones in modulating myocardial perfusion and coronary flow reserve. European Journal of Nuclear Medicine and Molecular Imaging, 2022, 49, 2209-2218.	6.4	6
2	What do we know about dynamic glucose-enhanced (DGE) MRI and how close is it to the clinics? Horizon 2020 GLINT consortium report. Magnetic Resonance Materials in Physics, Biology, and Medicine, 2022, 35, 87-104.	2.0	7
3	A genetically encoded sensor for in vivo imaging of orexin neuropeptides. Nature Methods, 2022, 19, 231-241.	19.0	50
4	Decoupling astrocytes in adult mice impairs synaptic plasticity and spatial learning. Cell Reports, 2022, 38, 110484.	6.4	43
5	Vascular Response to Spreading Depolarization Predicts Stroke Outcome. Stroke, 2022, 53, 1386-1395.	2.0	11
6	Direct vascular contact is a hallmark of cerebral astrocytes. Cell Reports, 2022, 39, 110599.	6.4	47
7	Measurement of cerebral oxygen pressure in living mice by two-photon phosphorescence lifetime microscopy. STAR Protocols, 2022, 3, 101370.	1.2	3
8	A FACED lift for cerebral blood flow imaging. Proceedings of the National Academy of Sciences of the United States of America, 2022, 119, .	7.1	3
9	Shear-stress sensing by PIEZO1 regulates tendon stiffness in rodents and influences jumping performance in humans. Nature Biomedical Engineering, 2021, 5, 1457-1471.	22.5	54
10	The severity of microstrokes depends on local vascular topology and baseline perfusion. ELife, 2021, 10, .	6.0	20
11	Distinct signatures of calcium activity in brain mural cells. ELife, 2021, 10, .	6.0	31
12	Diversity of neurovascular coupling dynamics along vascular arbors in layer II/III somatosensory cortex. Communications Biology, 2021, 4, 855.	4.4	23
13	SAFIR-I: Design and Performance of a High-Rate Preclinical PET Insert for MRI. Sensors, 2021, 21, 7037.	3.8	3
14	Fear learning induces α7-nicotinic acetylcholine receptor-mediated astrocytic responsiveness that is required for memory persistence. Nature Neuroscience, 2021, 24, 1686-1698.	14.8	31
15	Neutrophils Obstructing Brain Capillaries Are a Major Cause of No-Reflow in Ischemic Stroke. Cell Reports, 2020, 33, 108260.	6.4	129
16	DeepVesselNet: Vessel Segmentation, Centerline Prediction, and Bifurcation Detection in 3-D Angiographic Volumes. Frontiers in Neuroscience, 2020, 14, 592352.	2.8	83
17	Predicting Vessel Diameter Changes to Up-Regulate Biphasic Blood Flow During Activation in Realistic Microvascular Networks. Frontiers in Physiology, 2020, 11, 566303.	2.8	8
18	A complete pupillometry toolbox for real-time monitoring of locus coeruleus activity in rodents. Nature Protocols, 2020, 15, 2301-2320.	12.0	46

#	Article	IF	CITATIONS
19	Arousal-induced cortical activity triggers lactate release from astrocytes. Nature Metabolism, 2020, 2, 179-191.	11.9	82
20	Initial Characterization of the SAFIR Prototype PET-MR Scanner. IEEE Transactions on Radiation and Plasma Medical Sciences, 2020, 4, 613-621.	3.7	9
21	Structural basis of astrocytic Ca2+ signals at tripartite synapses. Nature Communications, 2020, 11, 1906.	12.8	133
22	A Bright and Colorful Future for G-Protein Coupled Receptor Sensors. Frontiers in Cellular Neuroscience, 2020, 14, 67.	3.7	35
23	Rapid Reconfiguration of the Functional Connectome after Chemogenetic Locus Coeruleus Activation. Neuron, 2019, 103, 702-718.e5.	8.1	198
24	Red blood cells stabilize flow in brain microvascular networks. PLoS Computational Biology, 2019, 15, e1007231.	3.2	41
25	In vivo imaging with a water immersion objective affects brain temperature, blood flow and oxygenation. ELife, 2019, 8, .	6.0	39
26	Oxyphor 2P: A High-Performance Probe for Deep-Tissue Longitudinal Oxygen Imaging. Cell Metabolism, 2019, 29, 736-744.e7.	16.2	105
27	Non-Canonical Control of Neuronal Energy Status by the Na+ Pump. Cell Metabolism, 2019, 29, 668-680.e4.	16.2	79
28	Vascular density and distribution in neocortex. NeuroImage, 2019, 197, 792-805.	4.2	86
29	Performance Measurements of the SAFIR Prototype Detector With the STiC ASIC Readout. IEEE Transactions on Radiation and Plasma Medical Sciences, 2018, 2, 250-258.	3.7	13
30	Cortical Circuit Activity Evokes Rapid Astrocyte Calcium Signals on a Similar Timescale to Neurons. Neuron, 2018, 98, 726-735.e4.	8.1	178
31	DCC Is Required for the Development of Nociceptive Topognosis in Mice and Humans. Cell Reports, 2018, 22, 1105-1114.	6.4	21
32	Fiber-optic implant for simultaneous fluorescence-based calcium recordings and BOLD fMRI in mice. Nature Protocols, 2018, 13, 840-855.	12.0	64
33	Long-term In Vivo Calcium Imaging of Astrocytes Reveals Distinct Cellular Compartment Responses to Sensory Stimulation. Cerebral Cortex, 2018, 28, 184-198.	2.9	86
34	CHIPS: an Extensible Toolbox for Cellular and Hemodynamic Two-Photon Image Analysis. Neuroinformatics, 2018, 16, 145-147.	2.8	31
35	Current technical approaches to brain energy metabolism. Glia, 2018, 66, 1138-1159.	4.9	40

Dual Ring Prototype Electronic System for the Small Animal Fast Insert for MRI. , 2018, , .

0

#	Article	IF	CITATIONS
37	Intravitreal AAV-Delivery of Genetically Encoded Sensors Enabling Simultaneous Two-Photon Imaging and Electrophysiology of Optic Nerve Axons. Frontiers in Cellular Neuroscience, 2018, 12, 377.	3.7	14
38	The Relation Between Capillary Transit Times and Hemoglobin Saturation Heterogeneity. Part 2: Capillary Networks. Frontiers in Physiology, 2018, 9, 1296.	2.8	19
39	The Relation Between Capillary Transit Times and Hemoglobin Saturation Heterogeneity. Part 1: Theoretical Models. Frontiers in Physiology, 2018, 9, 420.	2.8	21
40	The relative influence of hematocrit and red blood cell velocity on oxygen transport from capillaries to tissue. Microcirculation, 2017, 24, e12337.	1.8	47
41	Stabilizing <i>g</i> -States in Centrosymmetric Tetrapyrroles: Two-Photon-Absorbing Porphyrins with Bright Phosphorescence. Journal of Physical Chemistry A, 2017, 121, 6243-6255.	2.5	22
42	Depth-dependent flow and pressure characteristics in cortical microvascular networks. PLoS Computational Biology, 2017, 13, e1005392.	3.2	99
43	Two-Photon Absorbing Phosphorescent Metalloporphyrins: Effects of ï€-Extension and Peripheral Substitution. Journal of the American Chemical Society, 2016, 138, 15648-15662.	13.7	55
44	InÂVivo Evidence for a Lactate Gradient from Astrocytes to Neurons. Cell Metabolism, 2016, 23, 94-102.	16.2	437
45	A Probable Dual Mode of Action for Both L- and D-Lactate Neuroprotection in Cerebral Ischemia. Journal of Cerebral Blood Flow and Metabolism, 2015, 35, 1561-1569.	4.3	77
46	Design and performance of an ultra-flexible two-photon microscope for in vivo research. Biomedical Optics Express, 2015, 6, 4228.	2.9	55
47	Deviant Processing in the Primary Somatosensory Cortex. Cerebral Cortex, 2015, 27, bhv283.	2.9	28
48	The Astrocyte: Powerhouse and Recycling Center. Cold Spring Harbor Perspectives in Biology, 2015, 7, a020396.	5.5	127
49	The impact of capillary dilation on the distribution of red blood cells in artificial networks. American Journal of Physiology - Heart and Circulatory Physiology, 2015, 308, H733-H742.	3.2	48
50	A dynamic model of oxygen transport from capillaries to tissue with moving red blood cells. American Journal of Physiology - Heart and Circulatory Physiology, 2015, 308, H206-H216.	3.2	50
51	Channel-Mediated Lactate Release by K <sup>+</sup> -Stimulated Astrocytes. Journal of Neuroscience, 2015, 35, 4168-4178.	3.6	163
52	Sparse, reliable, and long-term stable representation of periodic whisker deflections in the mouse barrel cortex. NeuroImage, 2015, 115, 52-63.	4.2	26
53	NH4+ triggers the release of astrocytic lactate via mitochondrial pyruvate shunting. Proceedings of the National Academy of Sciences of the United States of America, 2015, 112, 11090-11095.	7.1	67
54	Joint 3-D vessel segmentation and centerline extraction using oblique Hough forests with steerable filters. Medical Image Analysis, 2015, 19, 220-249.	11.6	74

#	Article	IF	CITATIONS
55	How doth the little busy bee: unexpected metabolism. Trends in Neurosciences, 2015, 38, 1-2.	8.6	21
56	Tactile frequency discrimination is enhanced by circumventing neocortical adaptation. Nature Neuroscience, 2014, 17, 1567-1573.	14.8	65
57	Two-photon microscopy with double-circle trajectories for in vivo cerebral blood flow measurements. Experiments in Fluids, 2013, 54, 1.	2.4	7
58	Novel two-alternative forced choice paradigm for bilateral vibrotactile whisker frequency discrimination in head-fixed mice and rats. Journal of Neurophysiology, 2013, 109, 273-284.	1.8	59
59	Topology and Hemodynamics of the Cortical Cerebrovascular System. Journal of Cerebral Blood Flow and Metabolism, 2012, 32, 952-967.	4.3	109
60	Reorganization of cortical population activity imaged throughout long-term sensory deprivation. Nature Neuroscience, 2012, 15, 1539-1546.	14.8	193
61	<i>In Vivo</i> Evidence for Lactate as a Neuronal Energy Source. Journal of Neuroscience, 2011, 31, 7477-7485.	3.6	353
62	Vascularization of Cytochrome Oxidase-Rich Blobs in the Primary Visual Cortex of Squirrel and Macaque Monkeys. Journal of Neuroscience, 2011, 31, 1246-1253.	3.6	39
63	Metabotropic glutamate receptor mGluR5 is not involved in the early hemodynamic response. Journal of Cerebral Blood Flow and Metabolism, 2011, 31, e1-e10.	4.3	39
64	Assessment of brain responses to innocuous and noxious electrical forepaw stimulation in mice using BOLD fMRI. Pain, 2010, 151, 655-663.	4.2	64
65	Stimulation-Induced Increases of Astrocytic Oxidative Metabolism in Rats and Humans Investigated with 1- <sup>11</sup> C-Acetate. Journal of Cerebral Blood Flow and Metabolism, 2009, 29, 44-56.	4.3	43
66	A beta-scintillator for surface measurements of radiotracer kinetics in the intact rodent cortex. NeuroImage, 2009, 48, 339-347.	4.2	6
67	The Microvascular System of the Striate and Extrastriate Visual Cortex of the Macaque. Cerebral Cortex, 2008, 18, 2318-2330.	2.9	229
68	Quantitative evaluation of 11C-ABP688 as PET ligand for the measurement of the metabotropic glutamate receptor subtype 5 using autoradiographic studies and a beta-scintillator. NeuroImage, 2007, 35, 1086-1092.	4.2	37
69	Modeling the cerebral blood flow using a linear system approach. Proceedings in Applied Mathematics and Mechanics, 2007, 7, 4020027-4020028.	0.2	0
70	Constant-infusion H(2)15O PET and acetazolamide challenge in the assessment of cerebral perfusion status. Journal of Nuclear Medicine, 2004, 45, 1344-50.	5.0	11
71	Quantitative Cerebral Blood Flow Measurements in the Rat Using a Beta-Probe and H215O. Journal of Cerebral Blood Flow and Metabolism, 2003, 23, 1455-1460.	4.3	39
72	A femoral arteriovenous shunt facilitates arterial whole blood sampling in animals. European Journal of Nuclear Medicine and Molecular Imaging, 2002, 29, 319-323.	6.4	59

#	Article	IF	CITATIONS
73	Changes of Cerebral Blood Flow during Short-Term Exposure to Normobaric Hypoxia. Journal of Cerebral Blood Flow and Metabolism, 1998, 18, 906-910.	4.3	67
74	Monoamine oxidase B single-photon emission tomography with [ 123 I]Ro 43-0463: imaging in volunteers and patients with temporal lobe epilepsy. European Journal of Nuclear Medicine and Molecular Imaging, 1998, 25, 464-470.	6.4	16
75	Human hippocampus establishes associations in memory. Hippocampus, 1997, 7, 249-256.	1.9	277
76	Structural Basis of Astrocytic Ca <sup>2 </sup> Signals at Tripartite Synapses. SSRN Electronic Journal, 0, , .	0.4	2